Journal of
Applied Remote Sensing

RemoteSensing.SPIEDigitalLibrary.org

Validation of DigitalGlobe WorldView-3 Earth imaging satellite shortwave infrared bands for mineral mapping

Fred A. Kruse
William M. Baugh
Sandra L. Perry

SPIE.

Validation of DigitalGlobe WorldView-3 Earth imaging satellite shortwave infrared bands for mineral mapping

Fred A. Kruse,[a,*] **William M. Baugh,**[b] **and Sandra L. Perry**[c]
[a]Naval Postgraduate School, Physics Department and Remote Sensing Center, 833 Dyer Road, Monterey, California 93943, United States
[b]DigitalGlobe Inc., 1601 Dry Creek Drive, Suite 260, Longmont, Colorado 80503, United States
[c]Perry Remote Sensing, LLC, 9105 East Wesley Avenue, Denver, Colorado 80231, United States

Abstract. WorldView-3 (WV-3) is a newly launched (August 2014) high-spatial resolution commercial multispectral satellite sensor with eight visible to near-infrared bands (0.42 to 1.04 μm) and eight shortwave infrared (SWIR) bands (1.2 to 2.33 μm). Previous analyses using hyperspectral imagery (HSI) data of Cuprite, Nevada, to simulate WV-3's eight SWIR bands demonstrated identification and mapping of a wide variety of minerals, including kaolinite, alunite, buddingtonite, muscovite, calcite, and hydrothermal silica. These results, using partial unmixing, showed mineral occurrences similar to those mapped using full resolution HSI data and established WV-3's potential as a valuable new mineral mapping tool. Confusion matrix analyses using the HSI data as ground truth did indicate, however, some difficulties with mapping spectrally similar minerals using the multispectral data. Follow-up mineral mapping, using on-orbit WV-3 data acquired September 19, 2014, for Cuprite, Nevada, and the same algorithms and methods used for WV-3 simulation, indicates that the WV-3 sensor is performing as expected. WV-3 SWIR data analyses closely match expectations for mineral mapping as predicted by the simulation. While not as capable as an HSI sensor, WV-3's carefully selected eight SWIR bands provide new remote mineral mapping capabilities not available from any other spaceborne multispectral system. [DOI: 10.1117/1.JRS.9.096044]

Keywords: WorldView-3; shortwave infrared; multispectral mineral mapping; hyperspectral; Cuprite, Nevada alteration.

Paper 15233 received Mar. 24, 2015; accepted for publication Apr. 22, 2015; published online May 27, 2015.

1 Introduction

WorldView-3 (WV-3), launched August 13, 2014, is the latest in a constellation of commercial high-spatial resolution Earth imaging satellites developed by DigitalGlobe Inc. (Longmont, Colorado, USA). WorldView-1 (WV-1) was launched in 2007 with a panchromatic (PAN) imaging system capable of 0.5-m spatial resolution.[1] WorldView-2 (WV-2), launched in 2009, provides high-spatial resolution PAN data at a 0.46-m pixel size, plus visible and near-infrared (VNIR) imagery (0.4 to 1.04 μm) at a 1.85-m spatial resolution in eight multispectral bands.[2] WV-3 is an incremental improvement to the previous sensors, delivering essentially the same PAN and VNIR multispectral capabilities (albeit at 0.31- and 1.24-m spatial resolution, respectively).[3] These are supplemented on WV-3 by an additional eight shortwave infrared (SWIR) bands (referred to here as bands S1 to S8) ranging from approximately 1.2 to 2.33 μm at 3.7-m spatial resolution (though currently released only at 7.5-m spatial resolution).[3] The system also includes an additional 12 bands "Clouds, Aerosols, Water Vapor, Ice, and Snow" (CAVIS) at 30-m resolution for atmospheric compensation. Combined, these give WV-3 the distinction of having a total of 29 spectral bands, spanning the VNIR-SWIR range, and being the only commercial high-spatial resolution SWIR multispectral Earth imaging satellite currently in orbit.

---

*Address all correspondence to: Fred A. Kruse, E-mail: fakruse@nps.edu

This paper summarizes an assessment of using only the eight WV-3 SWIR bands for mineral mapping for a well-known site—Cuprite, Nevada. The Cuprite mining district is located about 200 km northwest of Las Vegas, Nevada, USA, along U.S. Highway 95. Surface geology at Cuprite consists of a variety of Cambrian—through Tertiary-age rocks, most notable for their extensive hydrothermal alteration[4–7] (Fig. 1). Cuprite has been used since the 1970s to validate multispectral and HSI remote sensing for mineralogical and geological mapping.[6–13]

An alteration map [Fig. 1(a)] compiled from a combination of airborne multispectral imagery, traditional field mapping, and laboratory measurements[6] and modified in presentation by the U.S. Geological Survey (USGS)[13] is shown to introduce alteration at Cuprite and for later reference. The three mapped zones (silicified, opalized, and argilized) are classic alteration descriptions that typically include mineral assemblages rather than a specific individual mineral. Silicified rocks are described as containing abundant quartz, chalcedony, minor alunite, and kaolinite, and some postalteration calcite.[6,13] Opalized rocks (opalite) contain opal with variable amounts of kaolinite and alunite, and minor calcite.[6,13] Argillized areas are typically within or adjacent to opalized zones and contain primary quartz, unaltered sanadine, opal, montmorillonite, and kaolinite.[6,13]

Produced from airborne visible/infrared imaging spectrometer (AVIRIS) data by the USGS,[13] Fig. 1(b) is a subset of the original image map, and provides a more detailed surface mineralogy reference. The USGS mineral map is a highly detailed compilation of surface minerals based on an expert system approach to HSI spectral feature and shape matching,[11] and is supported by field validation, x-ray diffraction, and laboratory spectral measurements.[13] The spectral map includes identification and mapping of several mineral groups, and information about mineral composition, crystallinity, and spectral mixing based on matching to specific library spectra.[13,14] While this provides extensive mineralogic information for Cuprite, note that most HSI algorithms do not map to this level of detail, so more general mineral classes are used in this study. Broader groups of key minerals are more typically identified, including kaolinites, alunites, buddingtonite, muscovites, carbonates, and certain types of silica. Note that most algorithms also map only the spectrally predominant mineral at each pixel. This is the approach adopted for our investigation.

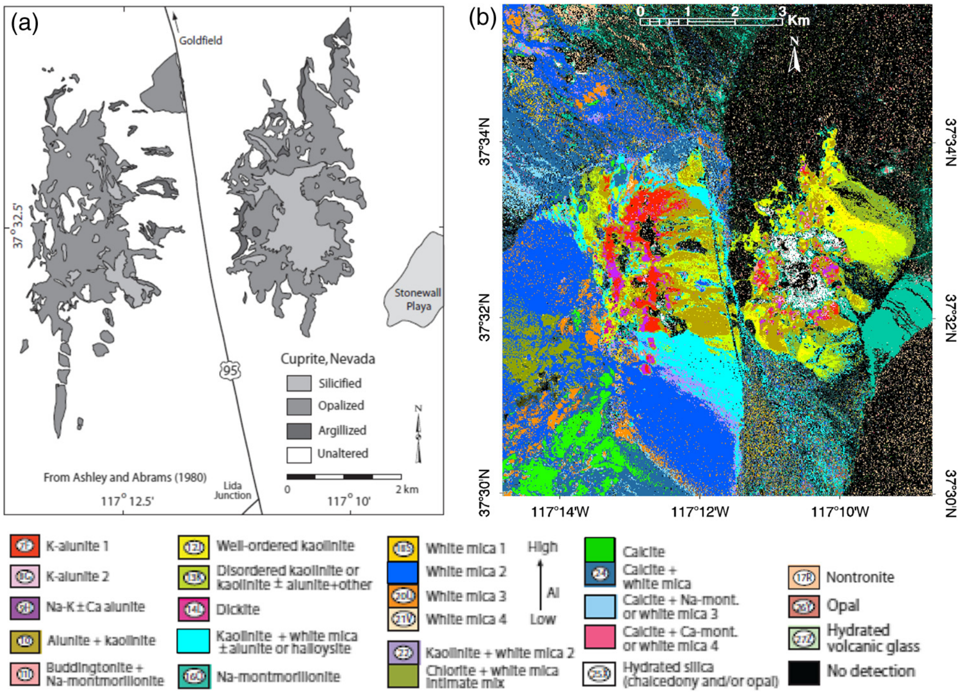

Fig. 1 (a) Cuprite field alteration map.[6] (b) U.S. Geological Survey (USGS) hyperspectral imagery mineral map of Cuprite.[13]

The results reported here are a follow-up to a previous study which utilized hyperspectral data to simulate WV-3 data and predict mineral mapping performance.[12,15] Mapping results for on-orbit WV-3 utilizing the exact same methodology and algorithms as those used in the simulation are reported and are directly compared to previous simulated WV-3 mineral mapping performance. Results indicate that the capability to map selected key minerals at Cuprite using WV-3 is similar to that predicted by simulation. Overall, on-orbit WV-3 SWIR data generally match mineral mapping as predicted by simulation and provide unprecedented high-spatial resolution and multispectral capabilities.

2 Previous WorldView-3 Simulation

Previous research predicting WV-3 capabilities for spectral mapping of mineralogy utilized AVIRIS data to simulate WV-3 SWIR data.[12,15] AVIRIS data were spectrally resampled to the proposed eight SWIR WV-3 bands at 3.7- and 7.5-m spatial resolution, and characteristic reflectance signatures extracted from the data for known mineral locations were used to map locations of specific minerals. Results demonstrated that WV-3 spectral bands should permit identification and mapping of certain key minerals; however, a potential exists for multispectral mapping errors for spectrally similar minerals.

2.1 *AVIRIS Data and Analysis*

AVIRIS radiance data collected by the Jet Propulsion Laboratory (JPL) on October 14, 2010, at 3-m spatial resolution for the Cuprite, Nevada, site were used as the starting point for the previously reported WV-3 SWIR simulation and mineral mapping.[12] AVIRIS is an imaging spectrometer [hyperspectral imaging (HSI) system], measuring radiance over the 0.4 to 2.5 μm range in 224 spectral bands at approximately 10-nm spectral resolution and variable spatial resolutions from approximately 2 to 20 m depending on flight altitude.[16,17] Eighty-six SWIR bands between

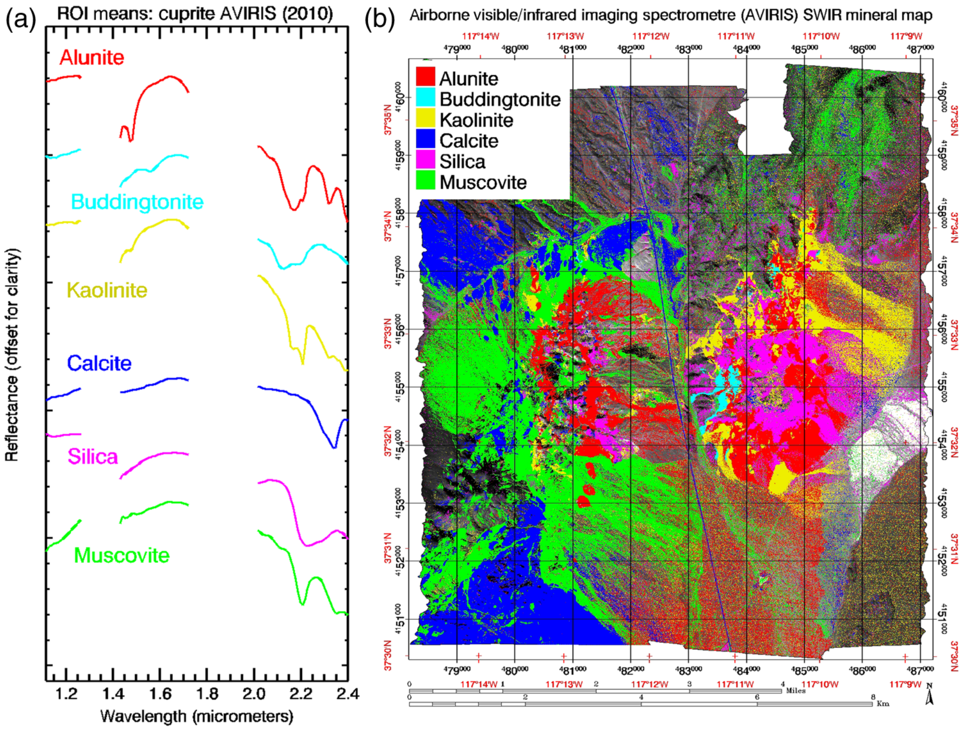

Fig. 2 (a) Mean shortwave infrared (SWIR) spectra extracted from the airborne visible/infrared imaging spectrometer (AVIRIS) data at 7.5-m spatial resolution for selected image regions of interest (ROI) with known mineralogy. (b) Mixture-tuned-matched filter (MTMF) mineral map showing spectrally predominant mineral for each AVIRIS pixel.[12]

approximately 1.2 and 2.5 μm with 3-m spatial resolution data were used for this analysis. The AVIRIS data were coregistered to orthorectified Advanced Spaceborne Thermal Emission and Reflection Radiometer (ASTER) imagery,[18,19] and resampled to both 3.7-m native WV-3 resolution, and the proposed WV-3 release spatial resolution of 7.5 m for analysis. The radiance data were corrected to apparent reflectance using the model-based "ACORN" atmospheric correction program[20] and further refined using field-measured calibration spectra.[21] This allows direct comparison to laboratory and field spectra (spectral libraries) using both visual and automated approaches.[22–29] Characteristic mean HSI reflectance signatures for laterally extensive minerals important to understand the general geology and hydrothermal alteration at Cuprite were extracted from the data for known mineral locations [Fig. 2(a)], and mapped using the mixture-tuned-matched filter (MTMF) partial unmixing algorithm[30–32] [Fig. 2(b)].

The AVIRIS data were analyzed using a standardized approach—linear transformation utilizing the minimum noise fraction transformation[33] to whiten noise, followed by MTMF.[30–32] Typically used for HSI data, this method locates known spectral signatures in the presence of a mixed or unknown background (Fig. 3). MTMF is also described as "partial unmixing," as it does not require knowledge of all of the spectral endmembers, thus each individual material can be separately unmixed without knowing the full background composition. MTMF combines the best attributes of the classic matched filter (MF)[34–36] with the feasibility constraints of spectral mixing.[37] It allows both determination of specific minerals and estimation of their pixel abundances by calculating two measures: an MF score and infeasibility score (Fig. 3).[32]

These two attributes are typically used together to determine occurrence and abundance of a particular material at each pixel of a spectral image dataset. The MF score determines the spectral abundance of the material, while the infeasibility score determines whether the measurement is a feasible mixture of background and the target signature. Two-dimensional scatter plotting is usually used to highlight feasible mixtures; however, this is somewhat subjective. For the purposes of this research, an "MTMF Feasibility Ratio"[38] (MF score/infeasibility score) was used for standardization between the datasets. All data analyzed utilizing MTMF were thresholded to show only the best mineral match (one material per pixel) for MTMF feasibility ratios greater than 0.025. AVIRIS results are presented for the spectrally predominant minerals only [Fig. 2(b)] to facilitate later comparison with the simulated WV-3 data. Mineral classes mapped using AVIRIS generally correspond with the main mineral groups and locations shown in previously published alteration maps[5,6] and HSI-derived mineral maps[7–13] (Fig. 1). The same MTMF mapping approach was applied to AVIRIS data and simulated WV-3 data,[12] and subsequently to the on-orbit WV-3 data for consistency.

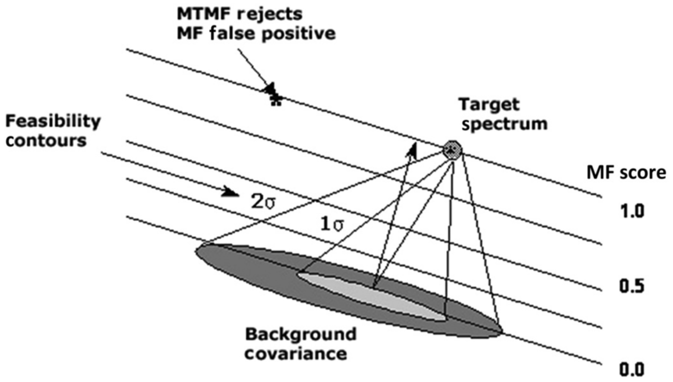

Fig. 3 MTMF concept showing identification and quantification of a known target spectrum in the presence of a diverse background. Higher MF scores (from 0.0 to 1.0 = 0% to 100% abundance) indicate that there is more of the target spectrum material in the pixel of interest. Lower infeasibility scores [forming 1σ and 2σ (etc.) cones extending from the background to the target] constrain the spectral signature in the context of mixing of the background and target signature. The best spectral matches can be mapped based on meeting the combined criteria of high MF score and low infeasibility score.[32]

2.2 *WV-3 Simulation and Results*

Simulated WV-3 SWIR bandpass functions were built based on specifications and generic response functions provided by DigitalGlobe (DG) (Table 1).[39] AVIRIS reflectance data were spectrally resampled to the WV-3 bands using the simulated bandpasses, which were nominally similar to those measured for the actual WV-3 system launched into orbit in 2014 (Table 1 and Fig. 4).[40] The spectrally simulated WV-3 data were then resized to 3.7- and 7.5-m spatial resolution using pixel aggregation (averaging). The 7.5-m data were used for subsequent analyses.

Mean SWIR reflectance spectra for selected minerals were extracted from the simulated WV-3 data based on known field locations (same locations as for the AVIRIS data) [Fig. 5(a)]. The spectral signatures were used to perform MTMF to match spectral signatures and map spatial locations [Fig. 5(b)]. Results were visually compared to AVIRIS mean spectra and mapping (Fig. 2).

Despite numerous remote sensing campaigns at Cuprite, no fully validated ground truth exists for the site—in fact, HSI data provide the best, most detailed mineral maps available [Fig. 1(b)].[13] Mineral classes mapped using AVIRIS, as part of this research, generally correspond with the main mineral groups and locations shown in previously published alteration maps[5,6] and HSI-derived mineral maps[7–13] (Fig. 1). For the purposes of this validation, the AVIRIS mineral map described here and shown in Fig. 2(b) was used as surrogate ground truth to evaluate WV-3 performance. These data were directly comparable in spectral and spatial

Table 1 Comparison of simulated WV-3 shortwave infrared (SWIR) bands versus on-orbit WV-3 SWIR. Full on-orbit WV-3 band responses (measured prelaunch) are shown in Fig. 4.

SWIR ID	WV-3 (Simulated)	WV-3 (On-Orbit)
Band S1	1.2097	1.2091
Band S2	1.5695	1.5716
Band S3	1.6495	1.6611
Band S4	1.7295	1.7295
Band S5	2.1645	2.1637
Band S6	2.2045	2.2022
Band S7	2.2594	2.2593
Band S8	2.3291	2.3292

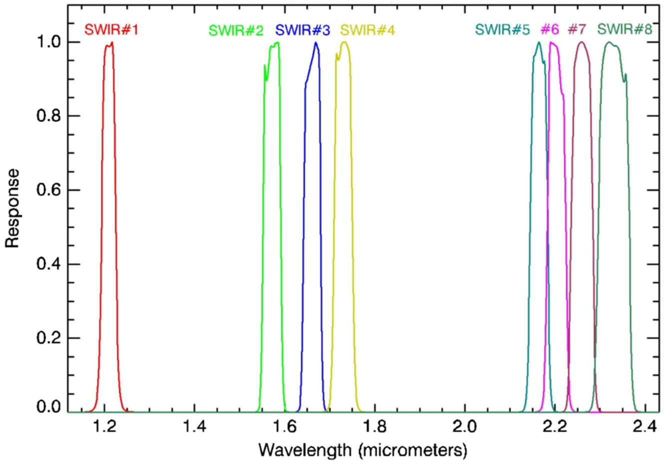

Fig. 4 WorldView-3 SWIR band responses (September 26, 2013).

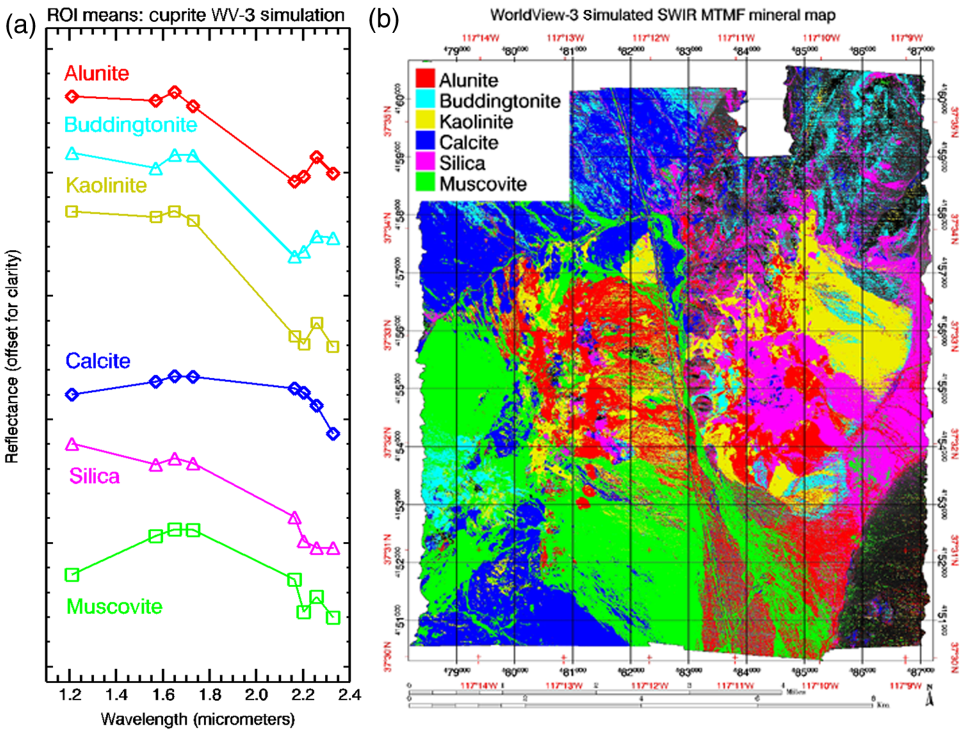

Fig. 5 (a) Mean reflectance spectra extracted from simulated WV-3 SWIR data at 7.5-m spatial resolution for selected image ROIs with known mineralogy. (b) MTMF mineral map showing spectrally predominant mineral for each simulated WV-3 pixel.[12] Visually compare to Fig. 2 AVIRIS results.

Table 2 Confusion matrix and supporting statistics comparing WV-3 simulated results (vertical axis) to airborne visible/infrared imaging spectrometer (AVIRIS) mixture-tuned-matched filter (MTMF) results (horizontal axis). Accuracy 50.92% and Kappa = 0.3843.

Class	Unclass	Alunite	Budd.	Kaolinite	Calcite	Silica	Musov	Total
Unclass	**45.39**	16.92	1.21	18.50	2.61	10.73	11.44	28.11
Alunite	4.30	**34.69**	0.26	3.55	2.06	0.32	3.75	7.45
Budd.	13.72	4.20	**73.54**	8.91	2.23	9.39	3.51	9.30
Kaolinite	6.24	14.14	20.76	**46.84**	4.03	8.49	14.47	11.55
Calcite	11.46	5.34	0.71	6.53	**82.44**	0.50	5.79	15.60
Silica	10.13	6.77	3.26	7.08	2.31	**67.93**	5.13	10.89
Muscov.	8.56	17.95	0.26	8.59	4.31	2.65	**55.90**	17.10
Total	100.00	100.00	100.00	100.00	100.00	100.00	100.00	100.00

Class	Commission (%)	Omission (%)	Prod acc (%)	User acc (%)
Unclass	22.13	54.41	45.59	77.87
Alunite	42.75	65.31	34.69	57.25
Budd.	97.46	26.46	73.54	2.54
Kaolinite	70.28	53.16	46.84	29.72
Calcite	49.10	17.56	82.44	50.90
Silica	67.31	32.07	67.93	32.69
Muscovite	43.86	44.10	55.90	56.14

Note: bold values represent correlation between WV-3 simulated results and AVIRIS results for each mineral.

coverage and spatial resolution. Visual comparison of the two mineral maps indicates a good correspondence [Figs. 2(b) and 5(b)]. A confusion matrix[41] computed using the AVIRIS as "ground truth" and evaluated with respect to mapping specific alteration minerals using the simulated WV-3 data,[12] however, shows that the overall accuracy is 50.92% and the per-pixel match between the AVIRIS and WV-3 mineral mapping results using the Kappa coefficient[42,43] is 0.38 (Table 2). The simulated WV-3 data performed best for identification and mapping of buddingtonite, calcite, and silica according to the diagonals of the confusion matrix. Assessment of the errors of commission and omission in Table 2 and the AVIRIS and simulated WV-3 mineral maps illustrate, however, that the simulation mapped a large amount of buddingtonite, where the AVIRIS data did not [Figs. 2(b) and 5(b)]. Table 2 also illustrates that significant portions of the errors for all classes are attributable to unclassified areas, indicating that rather than misidentification of materials, many of the errors are ones where no identification was possible using the multispectral data, presumably because the simulated WV-3 data cannot resolve key spectral features because of lower spectral resolution. Additionally, Table 2 shows that there is significant confusion between alunite, kaolinite, and muscovite as well as between buddingtonite and kaolinite at simulated WV-3 bandpasses and spectral resolution.

Excluding unclassified pixels from the confusion matrix analysis improves the overall accuracy to 63.43% and the Kappa coefficient to 0.54 (Table 3). Confusion matrix diagonals are somewhat improved, and errors of commission and omission are more easily evaluated with respect to specific minerals. Buddingtonite, kaolinite, and silica are most often mapped as another mineral. AVIRIS pixels containing alunite, kaolinite, and muscovite are most often missing from the simulated WV-3 MTMF mapping.

Table 3 Confusion matrix and supporting statistics comparing WV-3 simulated results (vertical axis) to AVIRIS MTMF results (horizontal axis). Unclassified omitted. Accuracy 63.43% and Kappa = 0.5406.

Class	Unclass	Alunite	Budd.	Kaolinite	Calcite	Silica	Musov	Total
Unclass								
Alunite		**41.75**	0.26	4.36	2.12	0.35	4.23	11.76
Budd.		5.06	**74.44**	10.94	2.29	10.52	3.96	5.94
Kaolinite		17.02	21.01	**57.47**	4.14	9.51	16.34	18.70
Calcite		6.42	0.72	8.01	**84.65**	0.56	6.54	22.06
Silica		8.14	3.30	8.69	2.37	**76.09**	5.80	13.17
Muscov.		21.60	0.26	10.53	4.43	2.97	**63.13**	28.38
Total		100.00	100.00	100.00	100.00	100.00	100.00	100.00

Class	Commission (%)	Omission (%)	Prod acc (%)	User acc (%)
Unclass				
Alunite	20.80	58.25	41.75	79.20
Budd.	91.30	25.56	74.44	8.70
Kaolinite	59.88	42.53	57.47	40.12
Calcite	21.37	15.35	84.65	78.63
Silica	40.91	23.91	76.09	59.09
Muscovite	26.10	36.87	63.13	73.90

Note: bold values represent correlation between WV-3 simulated results and AVIRIS results for each mineral.

Some minerals are better separated by the WV-3 SWIR bands than others. Examination of the confusion matrices shows that performance is high for calcite, buddingtonite, and silica. There is still, however, confusion between minerals with similar SWIR spectral features such as alunite, kaolinite, and muscovite, which at high spectral resolution all have characteristic spectral features near 2.2 μm [Fig. 2(a)].

3 On-Orbit WV-3: Empirical Line Reflectance, Mineral Mapping, and Comparisons

WV-3 data of the Cuprite site were acquired September 19, 2014, at 3.7-m spatial resolution. SWIR data were prepared for release by DG at 7.5-m spatial resolution and stacked with the 1.6-m resolution VNIR bands using nearest neighbor resampling, providing a 16 band data cube. The full dataset was corrected to reflectance by DG using an empirical line correction[44,45] of WV-3 radiance data to October 2010 HSI AVIRIS reflectance data. AVIRIS data were previously corrected to reflectance using the model-based "FLAASH" atmospheric correction.[46] FLAASH-corrected AVIRIS reflectance spectra of bright and dark in-scene targets (playa and basalt, respectively) were used with WV-3 spectra for the same areas/materials to perform a linear regression (empirical line correction, calculating, and applying gains and offsets), converting radiance for each WV-3 band to match the known AVIRIS reflectance. (Note that DG plans to implement a WV-3 atmospheric-model-based reflectance correction, taking advantage of the WV-3 aerosol and water vapor CAVIS bands; however, this correction was not available to apply to the data used in this investigation.) Representative reflectance spectra were then extracted from the WV-3 SWIR reflectance data for known minerals using the same locations defined for both AVIRIS and simulated WV-3 analyses. MTMF mineral mapping was applied using the standardized approach, and the on-orbit WV-3 mapping results were compared to the AVIRIS mineral mapping results and the previous WV-3 simulation.

3.1 *Comparison of SWIR Imagery*

SWIR color composites were generated from the AVIRIS data, the simulated WV-3 data, and the on-orbit WV-3 data using bands at approximately 1.65, 2.20, and 2.33 μm (RGB) (Fig. 6). Potentially altered areas are shown on the images as magenta to red pixels. Based on known mineralogy, the alteration mineral alunite (absorption feature near 2.16 μm) appears dark magenta, whereas areas with argillic (high kaolinite content) alteration and muscovite (absorption features near 2.2 μm) occur as more pure red (pink) colors. Note the close visual match between AVIRIS, simulated WV-3, and on-orbit WV-3 color composites (Fig. 6).

3.2 *Comparison of Mean Image Spectra for Known Locations*

Mean SWIR reflectance spectra extracted from all three datasets for the previously defined regions of interest (ROI) show a close correspondence between the AVIRIS spectra, the

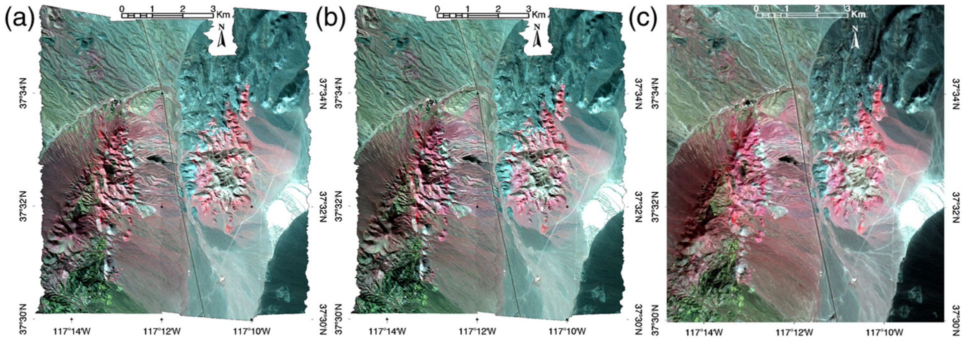

Fig. 6 SWIR color composite images using (a) AVIRIS bands 137, 194, 207 (1.652, 2.198, 2.327 μm) as RGB, (b) WV-3 simulated data using SWIR bands S3, S6, S8 (1.65, 2.20, 2.33 μm) as RGB, and (c) on-orbit WV-3 data using bands S3, S6, S8 (1.661, 2.202, 2.329 μm) as RGB.

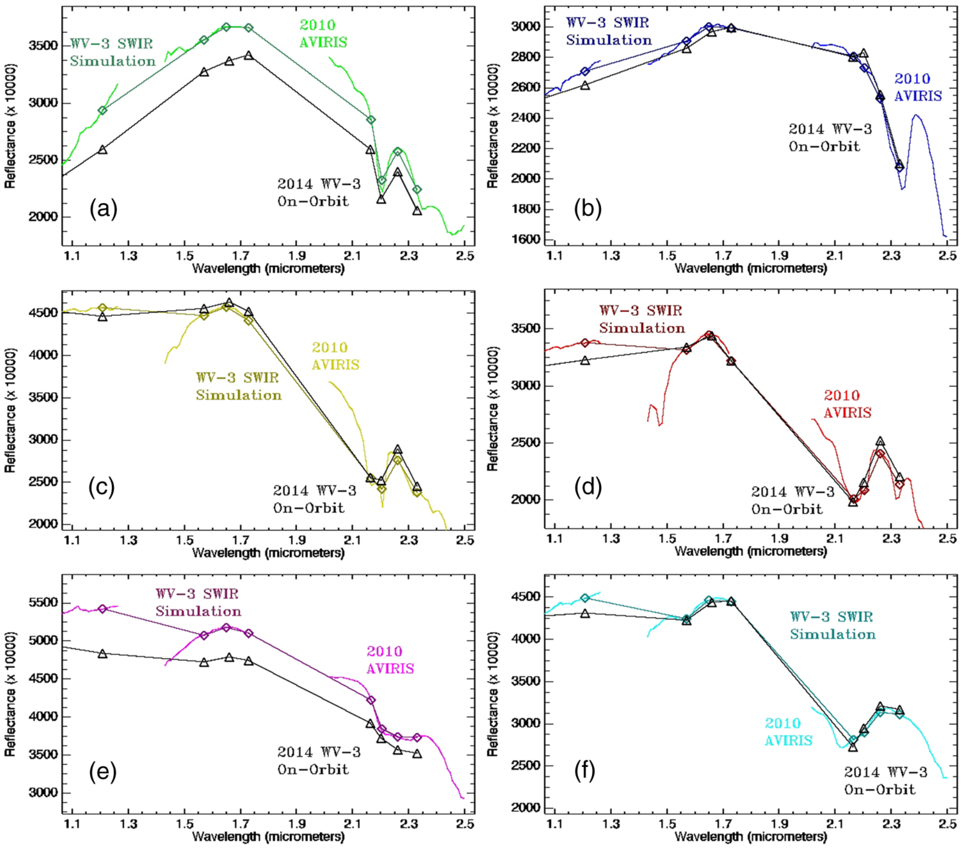

Fig. 7 Comparison of mean SWIR reflectance spectra extracted from the three datasets (AVIRIS, WV-3 simulated data, and on-orbit WV-3 data) for selected ROIs with known mineralogy: (a) muscovite, (b) calcite, (c) kaolinite, (d) alunite, (e) hydrothermal silica, and (f) buddingtonite. Note that colored symbols indicate the simulated WV-3 spectra, which are nearly identical to the AVIRIS spectra where they overlap, but with fewer bands.

simulated WV-3 spectra, and the actual WV-3 spectra (Fig. 7). All spectra have the expected shapes and show key absorption features, with less than 5% error in all cases. Nearly all of the spectra agree to within about 2%. Clearly, on-orbit WV-3 spectra delineate the mineralogy at Cuprite, exhibiting spectra very similar to those predicted in the WV-3 simulation using AVIRIS HSI data. Specific key features present in the WV-3 spectra include the 2.2 and 2.3 μm absorption features in muscovite [Fig. 7(a)], the 2.33 μm feature in calcite [Fig. 7(b)], the asymmetrical 2.2 μm feature in kaolinite [Fig. 7(c)], the 2.16 μm feature in alunite [Fig. 7(d)], and the broad hydrothermal silica shoulder feature near 2.25 μm [Fig. 7(e)]. The buddingtonite feature near 2.1 μm is still distinct, but is shifted to 2.2 μm because WV-3 does not include a specific band at 2.1 μm [Fig. 7(f)]. Together, these spectra form the basis of the MTMF mineral mapping for the Cuprite site.

3.3 *Comparison of MTMF Mineral Maps*

The on-orbit WV-3 reflectance spectra extracted for the previously defined ROI for selected minerals based on known field locations (Fig. 7) were used to perform MTMF to map the spatial locations of specific minerals [Fig. 8(c)]. This result was visually compared to the AVIRIS MTMF results [Fig. 8(a)] and simulated WV-3 MTMF mapping results [Fig. 8(b)]. The WV-3 on-orbit results [Fig. 8(c)] generally appear to match the simulated WV-3 mapping [Fig. 8(b)]. In some aspects, however, they actually appear to more closely match AVIRIS mapping (better performance than predicted). For example, it appears that the actual WV-3 sensor did a better job of mapping buddingtonite and kaolinite than that shown in the simulated results. Note that buddingtonite occurrences mapped by WV-3 are limited, and mostly correspond to

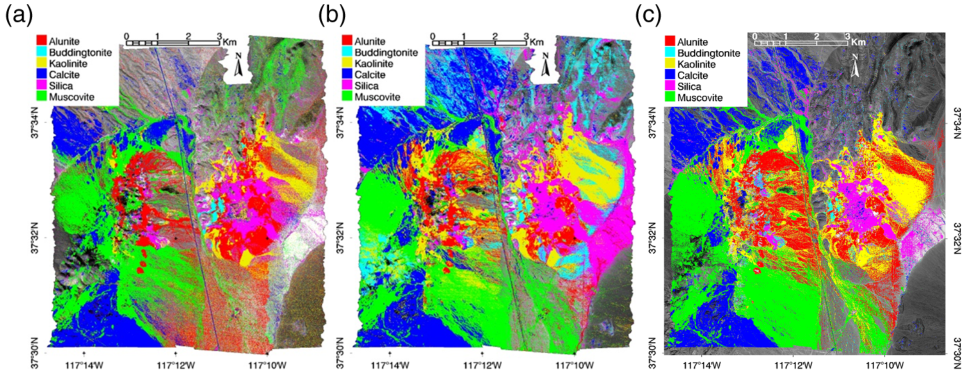

Fig. 8 (a) SWIR MTMF mineral mapping using AVIRIS, (b) WV-3 simulated data, and (c) on-orbit WV-3 data.

those shown in AVIRIS (cyan colored areas near the center of the left image), while the simulated WV-3 shows more extensive buddingtonite occurrences in areas known to be principally alunite or unclassified (cyan areas near top of center image and along right center edge, Fig. 8).

3.4 *Comparative Statistics*

Again, the AVIRIS HSI data provide the best, most detailed mineral maps available for the Cuprite site.[13] Comparison of the AVIRIS and on-orbit WV-3 MTMF mineral maps illustrates that mapped mineral classes generally correspond with main mineral groups and locations shown

Table 4 Confusion matrix and supporting statistics comparing WV-3 results (on-orbit 2014) (vertical axis) to AVIRIS results (horizontal axis). Accuracy 55.90% and Kappa = 0.3902.

Class	Unclass	Alunite	Budd.	Kaolinite	Calcite	Silica	Musov	Total
Unclass	**65.63**	26.48	10.33	29.18	14.05	35.26	24.25	44.30
Alunite	7.13	**35.02**	13.07	13.41	2.86	4.48	6.30	10.35
Budd.	2.03	1.57	**36.72**	1.93	0.82	3.70	1.00	1.87
Kaolinite	4.72	16.97	36.67	**40.14**	4.36	15.71	9.97	10.37
Calcite	6.77	2.11	0.90	2.82	**62.52**	1.68	4.48	10.60
Silica	3.36	2.16	0.88	2.77	1.39	**36.71**	1.11	4.33
Muscov.	10.36	15.68	1.44	9.76	14.00	2.46	**52.88**	18.18
Total	100.00	100.00	100.00	100.00	100.00	100.00	100.00	100.00

Class	Commission (%)	Omission (%)	Prod acc (%)	User acc (%)
Unclass	28.88	34.37	65.63	71.12
Alunite	58.38	64.98	35.02	41.62
Budd.	93.70	63.28	36.72	6.30
Kaolinite	71.62	59.86	40.14	28.38
Calcite	43.19	37.48	62.52	56.81
Silica	55.60	63.29	36.71	44.40
Muscovite	50.05	47.12	52.88	49.95

Note: bold values represent correlation between on-orbit WV-3 results and AVIRIS results for each mineral.

in previously published alteration maps[5,6] and HSI-derived mineral maps.[7–13] The AVIRIS mineral map shown in Fig. 2(b) and again in Fig. 8(a) provided surrogate ground truth to evaluate the WV-3 performance [Fig. 8(c)]. Confusion matrices were computed using AVIRIS as ground truth and evaluated for mapping each specific alteration mineral. The overall performance of WV-3 on-orbit (Table 4) appears similar to that predicted by the WV-3 simulation (Table 2). While visual comparison of the two mineral maps suggests good correspondence, closer inspection and analysis of the confusion matrices for these data (Table 4) demonstrates an overall accuracy of 55.90% and the per-pixel match between AVIRIS and WV-3 mineral mapping results using the Kappa coefficient[42,43] is 0.39. The on-orbit WV-3 data performed best for identification and mapping of calcite and muscovite according to confusion matrix diagonals. Further assessment of errors of commission and omission indicates that WV-3 mapped a greater amount of buddingtonite compared to AVIRIS. This was less severe for the on-orbit WV-3 mapping, with only 16,263 pixels (2%) mapped as buddingtonite when they should have been unclassified, compared to the simulated WV-3 map of 109,847 pixels (14%) as buddingtonite that were unclassified on the AVIRIS mineral map. On-orbit WV-3 also exhibited considerable errors of commission for kaolinite and alunite mineral mapping. Most errors were caused by mapping unclassified AVIRIS pixels as specific minerals by WV-3 (Table 4). Overall, WV-3 illustrated serious errors of omission with respect to nearly all minerals mapped, indicating that, in many cases, no identification was possible using the multispectral data and the MTMF approach. These errors are similar to those observed in the WV-3 simulation. Table 4 shows that at the actual WV-3 bandpasses and spectral resolution, significant mineral mapping confusion exists between alunite, kaolinite, and muscovite. This is most prevalent in alluvial fan areas, where mixing occurs between all three minerals. Additional confusion exists between

Table 5 Confusion matrix and supporting statistics comparing WV-3 results (on-orbit 2014) (vertical axis) to AVIRIS (horizontal axis). Unclassified pixels omitted. Accuracy 62.23% and Kappa = 0.5122.

Class	Unclass	Alunite	Budd.	Kaolinite	Calcite	Silica	Musov	Total
Unclass								
Alunite		**47.64**	14.58	18.94	3.33	6.92	8.32	17.67
Budd.		2.14	**40.95**	2.72	0.95	5.72	1.32	2.29
Kaolinite		23.08	40.89	**56.68**	5.07	24.26	13.16	20.67
Calcite		2.88	1.00	3.98	**72.24**	2.60	5.91	18.74
Silica		2.93	0.98	3.91	1.62	**56.71**	1.47	6.94
Muscov.		21.33	1.60	13.77	16.29	3.79	**69.81**	33.69
Total		100.00	100.00	100.00	100.00	100.00	100.00	100.00

Class	Commission (%)	Omission (%)	Prod acc (%)	User acc (%)
Unclass				
Alunite	37.81	52.36	47.64	62.19
Budd.	86.86	59.05	40.95	13.14
Kaolinite	63.68	43.32	56.68	36.32
Calcite	18.05	27.26	72.74	81.95
Silica	29.26	43.29	56.71	70.74
Muscovite	31.24	30.19	69.81	68.76

Note: bold values represent correlation between on-orbit WV-3 results and AVIRIS results for each mineral.

buddingtonite and kaolinite, probably due to the fact that WV-3 does not have a spectral band that corresponds exactly to the buddingtonite absorption feature near 2.11 μm. Both results are similar to the previous WV-3 simulation.

Exclusion of unclassified pixels from the confusion matrix analysis for on-orbit WV-3 data improves both the overall accuracy to 62.23% and the Kappa coefficient to 0.51 (Table 5). Confusion matrix diagonals are significantly improved and errors of commission and omission are clarified with respect to specific minerals. As observed in the previous WV-3 simulation, buddingtonite, kaolinite, and silica are most often mapped as another mineral. Errors of omission, however, are generally higher for on-orbit WV-3 mineral mapping than indicated by simulation predictions.

3.5 *Other Approaches and Products*

Even though WV-3 is a multispectral sensor, we have compared its performance to the hyperspectral AVIRIS sensor and direct mineral mapping approaches to establish a baseline against HSI mineral mapping. This research establishes that, in fact, WV-3 can directly map some minerals based on their spectral signatures because of the well-designed placement of its SWIR bands. There are also other approaches well-suited to multispectral analysis that can produce unique and useful mapping products. A few selected examples shown here for WV-3 include spectral-based methods such as band ratios, directed color composite images, and mineral indices.

Color ratio composite images have long been used to highlight spectral signature shapes using multispectral data.[4,47–49] These are known to reduce the effects of shade, shadows, and image noise on classification. WV-3 VNIR reflectance ratios, in combination with the WV-3 S3/S5 (1.66/2.20 μm) ratio, provide legacy capabilities similar to Landsat color ratio composites that include the Thematic Mapper SWIR bands 5/7 (1.65/2.20 μm) ratio, but at much higher spatial resolution. This ratio generally allows mapping of clays and carbonates.[49] The well-placed WV-3 SWIR bands also provide a wide range of new possibilities for mapping key materials of interest for geologic and alteration mapping using band ratios. For example, WV-3 SWIR band ratios S5/S6 (2.16/2.20 μm) and S7/S6 (2.26/2.20 μm) used together highlight spectral absorption features at 2.2 μm. Band ratio S7/S8 (2.26/2.33 μm) in combination with band ratio S7/S6 (2.26/2.20 μm) accentuates the distribution of materials with absorption features near 2.33 μm and establishes a spectral slope for materials like alunite. Combining S5/S6, S7/S6, and S7/S8 ratios (RGB) as a color composite image allows mapping of materials like muscovite (light red), alunite and related minerals (blue-green), and carbonates (blue) [Fig. 9(a)]. The orange area right–center in the image corresponds to the distribution of hydrothermal silica. Other band ratios can be designed utilizing both VNIR and SWIR bands to highlight different minerals or specific materials, and to identify and/or mask areas of water or vegetation.

Directed color composites are simple three-band color images designed based on the known spectroscopic response of materials of interest. Key materials can be emphasized in specific colors by strategically selecting the three bands used for the RGB display based on spectral features and characteristics of the material(s) of interest. Using bands centered on a specific spectral absorption feature allows design of a color composite showing the desired material (s) in a predetermined color or range of colors. The vertical colored lines in the spectral plot [Fig. 9(b)] show the RGB bands used in the WV-3 directed color composite image of SWIR bands S5, S6, and S8 (2.16, 2.20, 2.33 μm) [Fig. 9(c)]. Image color saturation was enhanced using decorrelation stretching.[50] Muscovite appears red because of high SWIR band S5 (2.16 μm) reflectance coupled with low contributions of green and blue caused by absorption in SWIR band S6 (2.20 μm) and lower reflectance in SWIR band S8 (2.33 μm). Kaolinite is light magenta because of high contribution from SWIR band S5 (2.16 μm) in conjunction with some contribution of blue and green from SWIR bands S8 (2.33 μm) and S6 (2.20 μm), respectively. Carbonates (calcite) are yellow-green in Fig. 9(c) because of high reflectance in SWIR bands S5 (2.16 μm) and S6 (2.20 μm) and low reflectance in SWIR band S8 (2.33 μm) caused by the carbonate absorption feature near 2.33 μm. Alunite appears blue in the image because of higher reflectance near 2.33 μm compared to lower reflectance in SWIR bands S5 (2.16 μm) and S6 (2.20 μm). Other directed color composites can be designed to highlight specific materials, spectral shapes, or absorption features.

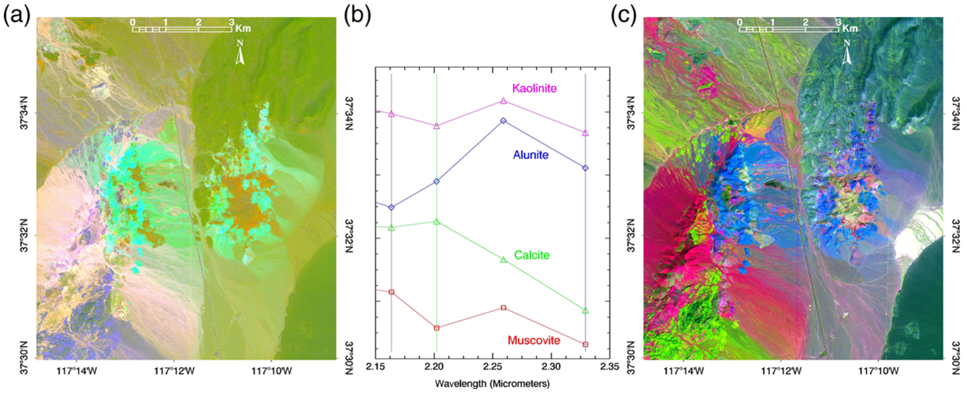

Fig. 9 (a) WV-3 SWIR reflectance band ratios S5/S6, S7/S6, S7/S8 (2.16/2.20 μm, 2.26/2.20 μm, 2.26/2.33 μm) as RGB, (b) selected representative WV-3 mineral spectra, and (c) directed color composite with SWIR bands S5, S6, and S8 (2.16, 2.20, 2.33 μm) as RGB. Color saturation of the right image was enhanced using decorrelation stretching[50] (hues remain unchanged). The vertical colored lines in the spectral plot (b) show the bands displayed as RGB in the directed color composite image (c). The spectral plots are used to design specific color ratios and directed color composites to show materials of interest in predetermined colors.

Indices for mapping spectral characteristics of materials using multispectral data have long been used for detection of vegetation (e.g., NDVI).[51–53] They have also been extensively used for geologic/mineral mapping with the ASTER sensor,[48,54,55] which had SWIR spectral bands similar to WV-3, but at a lower (30 m) spatial resolution. Mineral indices are typically more complex images than simple RGB color composites or band ratios. They are designed to show occurrence measures for specific minerals or groups of minerals. There are many possible combinations, several of which are shown in Fig. 10 to illustrate the WV-3 capabilities.

These alternative processing and analysis methods demonstrate the wealth of spectral information available in the WV-3 SWIR bands. They illustrate that the WV-3 data are equally amenable to mineral analysis using a wide variety of algorithms and methods developed for multispectral data analysis. In addition to unique SWIR bands, WV-3 provides matchless opportunities for fused VNIR-SWIR analysis and for PAN sharpening of results at an unprecedented 0.31-m spatial resolution.

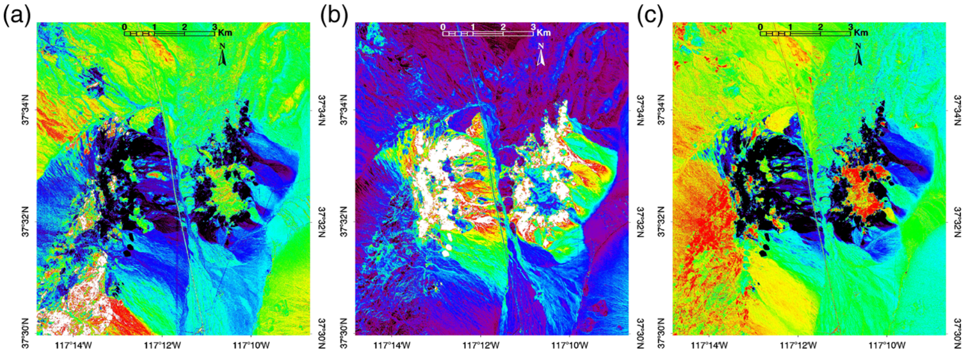

Fig. 10 Selected SWIR mineral indices derived from the on-orbit WV-3 data. (a) WV-3 carbonate index [defined here as WV-3 SWIR bands [S6/(S7 + S8)], or 2.20 μm/(2.26 μm + 2.33 μm)]: areas with carbonate signatures appear red or white. (b) Alunite/kaolinite/pyrophyllite index [defined by the USGS as a relative band depth (RBD) image[48] using ASTER bands (S4 + S6)/S5 and implemented here as WV-3 SWIR bands [(S3 + S6)/S5], or (1.66 μm + 2.20 μm)/2.16 μm]: areas with these minerals are green through white. (c) AL-OH group composition index [defined by CSIRO[55] as ASTER bands (S5 + S7)/S6 and adapted here to WV-3 SWIR bands (S5 + S7)/S6 or (2.16 μm + 2.26 μm)/2.20 μm]: blue is well ordered kaolinite or Al-rich white mica (muscovite, illite, paragonite, pyrophyllite, beidellite). Red is Al-poor (Si-rich) white mica (phengite), or montmorillonite.[55]

4 Conclusions

WV-3 is a highly capable commercial multispectral satellite sensor with an impressive combination of high-spatial resolution and key SWIR spectral bands. Previous simulation using AVIRIS data of Cuprite, Nevada, demonstrated that WV-3 should be able to identify and map selected minerals based on their SWIR spectral properties utilizing spectral matching approaches. MTMF mineral maps produced during the simulation showed similar mineral occurrences and spatial distributions to those mapped using full-resolution, 86-SWIR-band AVIRIS data. Statistical analyses using confusion matrices and AVIRIS data as ground truth, however, illustrated typical multispectral shortcomings (confusion between similar minerals), caused by reduced spectral resolution as compared to AVIRIS and with respect to key spectral features of minerals. Given that WV-3 is not a hyperspectral sensor and does not perform as such, simulated WV-3 mineral mapping results were promising, establishing WV-3's potential as valuable new tool for geologic and alteration mapping—better than any other commercial multispectral sensor currently in orbit.

Follow-up mineral mapping using actual on-orbit WV-3 data for Cuprite and the same algorithms and methods used for the simulation, indicates that the WV-3 sensor is performing as expected and predicted. Extracted spectra are remarkably similar to the simulated spectra with typically less than 5% error. Key mineral features are readily apparent in the on-orbit WV-3 spectra, and these were successfully used to map the character and distribution of alteration minerals at the Cuprite site using the MTMF approach. Minerals mapped included kaolinite, alunite, buddingtonite, muscovite, calcite, and hydrothermal silica. Overall, the on-orbit WV-3 SWIR data closely match expectations for mineral mapping as predicted by the simulation, and WV-3's carefully selected eight SWIR bands and 7.5-m resolution provide extensive new mineral mapping capabilities not available from other spaceborne multispectral systems.

In addition to the direct mineral mapping approaches described in the WV-3 simulation and validated against on-orbit WV-3 SWIR data, the unique selection of spectral bands provides SWIR multispectral mapping capabilities similar to those demonstrated by the ASTER sensor but at much higher spatial resolution. Approaches such as band ratios, directed color composites, and mineral indices can be used with WV-3 data along with direct mineral mapping methods and other multispectral algorithms to provide results unmatched by any current orbiting commercial sensor. With the ASTER SWIR bands now defunct; WV-3 is the only multispectral sensor currently in orbit with multiple, nearly contiguous, SWIR bands. It is clear that WV-3 will provide vastly improved capabilities in support of geologic and other surface mapping applications.

Acknowledgments

WV-3 data for the Cuprite site were calibrated to radiance, converted to reflectance, and provided by DigitalGlobe, Inc. AVIRIS data were acquired and processed to radiance by JPL. Use of brand names in this paper does not indicate endorsement by the United States Government.

References

1. DigitalGlobe Inc., "Worldview-1 specifications," https://www.digitalglobe.com/sites/default/files/WorldView1-DS-WV1.pdf (17 April 2015).
2. DigitalGlobe Inc., "Worldview-2 specifications," https://www.digitalglobe.com/sites/default/files/DG_WorldView2_DS_PROD.pdf (17 April 2015).
3. DigitalGlobe Inc., "Worldview-3 specifications," https://www.digitalglobe.com/sites/default/files/DG_WorldView3_DS_forWeb_0.pdf (17 April 2015).
4. L. C. Rowan et al., "Discrimination of rock types and detection of hydrothermally altered areas in south-central Nevada by the use of computer-enhanced ERTS images," U.S. Geological Survey Professional Paper 883, pp. 34 (1974).
5. M. J. Abrams et al., "Mapping of hydrothermal alteration in the Cuprite mining district, Nevada, using aircraft scanner images for the spectral region 0.46–2.36 micrometers," *Geology* **5**, 713–718 (1977).

6. R. P. Ashley and M. J. Abrams, "Alteration mapping using multispectral images—Cuprite mining district, Esmeralda County, Nevada," U.S. Geological Survey Open File Report 80-367, pp. 17 (1980).
7. G. A. Swayze, "The hydrothermal and structural history of the Cuprite Mining District, southwestern Nevada: an integrated geological and geophysical approach," unpublished Ph.D. Dissertation, Univ. of Colorado at Boulder, pp. 399, Boulder, Colorado (1997).
8. A. F. H. Goetz et al., "Imaging spectrometry for earth remote sensing," *Science* **228**, 1147–1153 (1985).
9. F. A. Kruse, K. S. Kierein-Young, and J. W. Boardman, "Mineral mapping at Cuprite, Nevada with a 63 channel imaging spectrometer," *Photogramm. Eng. Remote Sens.* **56**(1), 83–92 (1990).
10. L. C. Rowan and J. C. Mars, "Lithologic mapping in the Mountain Pass, California area using advanced spaceborne thermal emission and reflection spectrometer (ASTER) data," *Remote Sens. Environ.* **84**, 350–366 (2003).
11. R. N. Clark et al., "Imaging spectroscopy: earth and planetary remote sensing with the USGS Tetracorder and expert systems," *J. Geophys. Res.* **108**(E12) 5131 (2003).
12. F. A. Kruse and S. L. Perry, "Mineral mapping using simulated WorldView-3 short-wave-infrared imagery," *Remote Sens.* **5**(6), 2688–2703 (2013).
13. G. A. Swayze et al., "Mapping advanced argillic alteration at Cuprite, Nevada, using imaging spectroscopy," *Econ. Geol.* **109**(5), 1179–1221 (2014).
14. R. N. Clark et al., "USGS digital spectral library splib06a," U.S. Geological Survey, Digital Data Series 231 (2007).
15. F. A. Kruse and S. L. Perry, "Mineral mapping using simulated short-wave-infrared bands planned for DigtalGlobe WorldView-3," in *Proc. Imaging and Applied Optics Technical Digest*, 24–28 June 2012, Monterey, California, Paper RM3E.4.pdf (CD-ROM), Optical Society of America, Washington, D. C. (2012).
16. W. M. Porter and H. E. Enmark, "System overview of the airborne visible/infrared imaging spectrometer (AVIRIS)," *Proc. SPIE* **834**, 22–31 (1987).
17. R. Green, "AVIRIS and related 21st century imaging spectrometers for earth and space science," in *High Performance Computing in Remote Sensing*, pp. 335–358, Chapman and Hall/CRC Press, Boca Raton, Florida (2007).
18. A. B. Kahle et al., "The advanced spaceborne thermal emission and reflectance radiometer (ASTER)," *Int. J. Imaging Syst. Technol.* **3**, 144–156 (1991).
19. M. Abram et al., "The advanced spaceborne thermal emission and reflection radiometer (ASTER) after fifteen years: review of global products," *Int. J. Appl. Earth Obs. Geoinf.* **38**, 292–301 (2015).
20. F. A. Kruse, "Comparison of ATREM, ACORN, and FLAASH atmospheric corrections using low-altitude AVIRIS data of Boulder, Colorado," in *Proc. 13th JPL Airborne Geoscience Workshop*, JPL Publication 05-3, Jet Propulsion Laboratory, Pasadena, California (2004).
21. R. N. Clark et al., "Surface reflectance calibration of terrestrial imaging spectroscopy data," in *Proc. of the 11th Annual JPL Airborne Earth Science Workshop*, R. O. Green, Ed., JPL Publication 03-04, pp. 43–63, Jet Propulsion Laboratory, Pasadena, California (2002).
22. G. R. Hunt, "Spectral signatures of particulate minerals in the visible and near infrared," *Geophysics* **42**(3), 501–513 (1977).
23. G. R. Hunt and R. P. Ashley, "Spectra of altered rocks in the visible and near infrared," *Econ. Geol.* **74**(7), 1613–1629 (1979).
24. R. N. Clark and T. L. Roush, "Reflectance spectroscopy: quantitative analysis techniques for remote sensing applications," *J. Geophys. Res.* **89**(B7), 6329–6340 (1984).
25. F. A. Kruse, "Use of airborne imaging spectrometer data to map minerals associated with hydrothermally altered rocks in the northern Grapevine Mountains, Nevada and California," *Remote Sens. Environ.* **24**(1), 31–51 (1988).
26. R. N. Clark et al., "Mapping with imaging spectrometer data using the complete band shape least-squares algorithm simultaneously fit to multiple spectral features from multiple materials," in *Proc. of the Third Airborne Visible/Infrared Imaging Spectrometer (AVIRIS) Workshop*, JPL Publication 91-28, pp. 2–3, Jet Propulsion Laboratory, Pasadena, California (1991).

27. F. A. Kruse, A. B. Lefkoff, and J. B. Dietz, "Expert system-based mineral mapping in northern Death Valley, California/Nevada using the airborne visible/infrared imaging spectrometer (AVIRIS)," *Remote Sens. Environ.* **44**, 309–336 (1993).
28. R. N. Clark, "Spectroscopy of rocks and minerals, and principles of spectroscopy," Chapter 1 in *Manual of Remote Sensing, Remote Sensing for the Earth Sciences*, Vol. **3**, pp. 3–58, John Wiley and Sons, New York (1999).
29. F. A. Kruse, "Expert system analysis of hyperspectral data," *Proc. SPIE* **6966**, 69660Q (2008).
30. J. W. Boardman, "Leveraging the high dimensionality of AVIRIS data for improved subpixel target unmixing and rejection of false positives: mixture tuned matched filtering," in *Summaries of the Seventh Annual JPL Airborne Geoscience Workshop*, Jet Propulsion Laboratory, Pasadena, California (1998).
31. F. A. Kruse and S. L. Perry, "Improving multispectral mapping by spectral modeling with hyperspectral signatures," *J. Appl. Remote Sens.* **3**(1), 033504(2009).
32. J. W. Boardman and F. A. Kruse, "Analysis of imaging spectrometer data using N-dimensional geometry and a mixture-tuned matched filtering (MTMF) approach," *Trans. Geosci. Remote Sens.* **49**(11), 4138–4152 (2011).
33. A. A. Green et al., "A transformation for ordering multispectral data in terms of image quality with implications for noise removal," *IEEE Trans. Geosci. Remote Sens.* **26**(1), 65–74 (1988).
34. D. O. North, "An analysis of the factors which determine signal/noise discrimination in pulsed-carrier systems," *Proc. IEEE* **51**(7), 1016–1027 (1963).
35. J. Y. Chen and I. S. Reed, "A detection algorithm for optical targets in clutter," *IEEE Trans. Aerospace Electron. Syst.* **AES-23**(1), 46–59 (1987).
36. J. C. Harsanyi and C. I. Chang, "Hyperspectral image classification and dimensionality reduction: an orthogonal subspace projection approach," *IEEE Trans. Geosci. Remote Sens.* **32**, 779–785 (1994).
37. A. Plaza et al., "Foreword to the special issue on spectral unmixing of remotely sensed data," *Trans. Geosci. Remote Sens.* **49**(11), 4103–4109 (2011).
38. F. A. Kruse et al., "Effect of reduced spatial resolution on mineral mapping using imaging spectrometry—examples using HyspIRI-simulated data," *Remote Sens.* **3**(8), 1584–1602 (2011).
39. W. Baugh, personal communication, DigitalGlobe Inc., Longmont, Colorado (2013).
40. W. Baugh, personal communication, DigitalGlobe Inc., Longmont, Colorado (2015).
41. J. A. Richards and X. Jia, *Remote Sensing Digital Image Analysis*, 4th ed., pp. 359–388, Springer-Verlag, Berlin-Heidelberg (2006).
42. R. A. Monserud and R. Leemans, "Comparing global vegetation maps with the Kappa-statistic," *Ecol. Model.* **62**, 275–293 (1992).
43. R. G. Congalton, "A review of assessing the accuracy of classifications of remotely sensed data," *Remote Sens. Environ.* **37**, 35–46 (1991).
44. D. A. Roberts, Y. Yamaguchi, and R. Lyon, "Comparison of various techniques for calibration of AIS data," in *Proc. of the 2nd Airborne Imaging Spectrometer Data Analysis Workshop*, JPL Publication 86-35, pp. 21–30, Jet Propulsion Laboratory, Pasadena, California (1986).
45. B.-C. Gao et al., "Atmospheric correction algorithms for hyperspectral remote sensing data of land and ocean," *Remote Sens. Environ.* **113**, 517–524 (2009).
46. M. W. Matthew et al., "Atmospheric correction of spectral imagery: evaluation of the FLAASH algorithm with AVIRIS data," *Proc. SPIE* **5093**, 474–482 (2003).
47. L. C. Rowan, A. F. H. Goetz, and R. P. Ashley, "Discrimination of hydrothermally altered rocks and unaltered rocks in visible and near infrared multispectral images," *Geophysics* **42**, 522–535 (1977).
48. J. C. Mars and L. C. Rowan, "Regional mapping of phyllic- and argillic-altered rocks in the Zagros magmatic arc, Iran, using advanced spaceborne thermal emission and reflection radiometer (ASTER) data and logical operator algorithms," *Geosphere* **2**(3), 161–186 (2006).
49. F. F. Sabins, *Remote Sensing: Principles and Interpretation*, 3rd ed., Waveland Press Inc., Long Grove, Illinois (2007).

50. A. R. Gillespie, A. B. Kahle, and R. E. Walker, “Color enhancement of highly correlated images I,” *Remote Sens. Environ.* **20**, 209–235 (1986).
51. J. W. Rouse et al., “Monitoring the vernal advancement and retrogradation (greenwave effect) of natural vegetation,” NASA/GSFC Type III Final Report, GSFC, Greenbelt, Maryland (1974).
52. R. D. Jackson, “Spectral indices in n-space,” *Remote Sens. Environ.* **13**, 409–421 (1983).
53. H. Nouri et al., “High spatial resolution WorldView-2 imagery for mapping NDVI and its relationship to temporal urban landscape evapotranspiration factors,” *Remote Sens.* **6** (2014).
54. T. Cudahy et al., “Satellite ASTER geoscience map of Australia version 1,” CSIRO Data Collection 10.4225/08/51400D6F7B335, Vol. 1, Geoscience Australia, Symonston, Australia (2012).
55. T. Cudahy, “Australian ASTER geoscience product notes, version 1,” CSIR0 ePublish No. EP-30-07-12-44, Vol. 1,Geoscience Australia, Symonston, Australia (2012).

Fred A. Kruse received his PhD in geology from the Colorado School of Mines in 1987. He has been involved in remote sensing research and applications for over 30 years. Currently, he is a research professor at the Naval Postgraduate School, teaching spectral remote sensing and synthetic aperture radar. His research explores the distribution and character of earth surface materials. He is also one of the scientists that originally developed the image analysis software ENVI.

William M. Baugh is a senior scientist at DigitalGlobe. He received an MS degree in geology from the University of Colorado, Boulder, USA, in 1995. He previously worked as an associate scientist at the National Center for Atmospheric Research and for over 15 years total in industry. His current focus is on leveraging WorldView-3’s new spectral capabilities to create practical applications. Additional interests include hyperspectral data, spectrometry, algorithm development, field research, radiometric calibration, and atmospheric compensation.

Sandra L. Perry is an exploration geologist specializing in satellite imagery analysis. She received a BS degree in geology from Indiana State University, specializing in structural and photogeology. After receiving her MS degree in geology at the Colorado School of Mines, she focused on digital image analysis of satellite data for mineral and hydrocarbon exploration worldwide. She has over 30 years of experience, participated on the ASTER Science Team, and was the lead scientist recommending WV-3 SWIR band designations.